

Analysis and Optimized CXL-Attached Memory Allocation for Long-Context LLM Fine-Tuning

Yong-Cheng Liaw, Shuo-Han Chen

Abstract—The growing prevalence of Large Language Models (LLMs) and their substantial memory requirements have prompted renewed interest in CPU offloading as a method to compensate for limited GPU memory. In particular, when CPU memory is leveraged to temporarily store intermediate states of LLMs, CPU memory becomes a new bottleneck and soon reaches the capacity limitation of commodity CPUs. In this work, we investigate the effectiveness of Compute Express Link (CXL) add-in card (AIC) memory as an extension to CPU memory, enabling larger model sizes and longer context lengths during fine-tuning. Through extensive benchmarking, this study quantifies the performance overhead introduced by transferring data between CXL memory, CPU, and GPUs, focusing on how concurrency and data volume influence bandwidth utilization and latency. This study also compares CPU-based optimizer steps when model parameters, gradients, and optimizer states reside in local memory versus CXL memory, revealing that naive adoption of CXL often degrades performance during the optimizer phase. To overcome these challenges, this study proposes a CXL-aware allocation to strategically partition CPU offloading workloads across both local and CXL memory. This study further demonstrates that employing multiple AICs significantly reduces bandwidth contention, thus improving scalability. Experimental results show that these optimizations enable efficient long-context LLM fine-tuning, underscoring CXL as a promising avenue for unlocking the full potential of CPU offloading in long-context LLM fine-tuning.

Index Terms—Compute Express Link, Memory Expansion, CPU offloading, Large Language Models, Training

I. INTRODUCTION

The rapid growth of Large Language Models (LLMs) and the ever-growing number of model parameters have introduced substantial challenges related to memory capacity [1]. As these models frequently exceed available GPU memory, performance bottlenecks arise during both training and deployment. Applications that require longer context lengths [2], such as long chain of thought [3, 4], generative agent [5], in-context learning [6], retrieval-augmented generation [7, 8], and multimodal tasks [9, 10], are experiencing rapid growth. To enhance performance in these scenarios, fine-tuning models on long-context datasets has become increasingly important [11–15]. However, such fine-tuning introduces substantial memory overhead, primarily due to the need to store intermediate activation values that scale proportionally to the context length [16–19]. Additionally, limited memory resources restrict the batch size for LLM training, consequently limiting achievable throughput. To address these constraints, especially in resource-limited environments, offloading strategies such as CPU offloading and solid-state drive (SSD) offloading have been proposed [20, 21]. While CPU offloading involves temporarily migrating LLM training or inference states from GPU to CPU (system) memory, SSD offloading further offloads these states onto SSDs, leveraging their larger and more cost-effective storage capacities. However, SSD offloading suffers from inherent performance and endurance limitations

associated with NAND flash memory. Consequently, CPU offloading has received significant attention [20, 22–24]. CPU offloading involves transferring memory components, including model parameters, gradients, optimizer states, and occasionally checkpointed activations, from limited GPU memory to larger-capacity system memory. Although CPU offloading enables the fine-tuning of larger models and supports longer context lengths on GPU-constrained systems, *the capacity of the system memory remains a significant challenge, particularly given the continuously growing model sizes and the demand for longer context and larger batch to improve throughput.*

System memory capacity is fundamentally limited by CPU specifications (e.g. 192 GB for most consumer grade CPUs [25]), available DIMM slots, and per-module DIMM capacity. To overcome these constraints, Compute Express Link (CXL) technology has emerged as a promising alternative, providing a viable solution to memory bottlenecks encountered during CPU offloading in LLM fine-tuning [26–28]. Leveraging the PCIe interface and high-performance DRAM, CXL provides a high-bandwidth, low-latency interconnect, enabling expansion of system memory capacity beyond traditional DIMM limitations without incurring the performance penalties of NAND flash-based SSDs. Specifically, CXL Type 3 devices facilitate memory expansion via add-in card (AIC) [29, 30], which are typically recognized by the host operating system as CPU-less Non-Uniform Memory Access (NUMA) nodes. Consequently, applications can access CXL-attached memory similarly to remote DRAM, albeit with distinct performance characteristics.

By utilizing CXL-attached memory, systems can support significantly larger memory footprints, effectively meeting the substantial memory requirements associated with fine-tuning long-context LLMs without resorting to costly high-capacity DIMMs or being constrained by limited DIMM slots [31]. However, *our findings demonstrate that naively integrating CXL-attached memory into existing CPU offloading workflows does not inherently ensure optimal performance.* Instead, this integration can introduce new performance issues, including data transfer overhead, bandwidth contention, and increased latency due to PCIe-based interconnections. This paper analyzes and strategically mitigates these performance bottlenecks, enabling effective utilization of CXL-attached memory to enhance CPU offloading performance in LLM fine-tuning.

CPU offloading techniques, such as ZeRO-Offload [20], temporarily store model parameters, gradients, and optimizer states from the GPU to the system memory (See Figure 1). While these techniques effectively reduce GPU memory consumption, they introduce frequent data transfers between the GPU and system memory. Additionally, CPU-based operations, like optimizer steps, become susceptible to transfer latency between the CPU

and system memory. When integrating CXL-attached memory as an extension or replacement for local DRAM, its distinct performance characteristics, particularly higher latency and differing bandwidth compared to local DIMMs, need to be carefully addressed [32]. Intuitive CXL integrations, including tiered memory system [33,34] or interleaving approach for CXL-attached memory [35], are typically implemented transparently at the Linux kernel level without requiring application-specific knowledge. Nonetheless, such general-purpose integrations often yield suboptimal performance when running specialized workloads. Consequently, custom CXL memory management policies explicitly tailored to the characteristics of long-context LLM fine-tuning workloads are necessary [36–38].

Studies have been proposed to explore CXL-attached memory for LLM workloads. For instance, Wang et al. [28] report the end-to-end performance of CPU offloading with CXL-attached memory and Tang et al. [39] leverage CXL-attached memory to store KV cache in LLM inference. Nonetheless, these studies primarily focus on characterizing general CXL-attached memory performance without analyzing details and proposing optimizations tailored specifically to CPU offloading workloads, resulting in a significant gap in understanding complex performance interactions such as frequent GPU-CPU data transfers, latency-sensitive CPU-based optimizer steps, and multi-GPU bandwidth contention on shared CXL AICs during long-context fine-tuning. To address these challenges, this study first performs benchmarking to quantify the performance overhead associated with utilizing CXL-attached memory in long-context CPU offloading scenarios. *The analysis identifies two primary performance bottlenecks.* The first bottleneck arises from significant performance degradation during CPU-based optimizer operations when model parameters, gradients, or optimizer states reside in higher latency CXL-attached memory rather than in local DRAM. The second bottleneck emerges from bandwidth contention when multiple GPUs simultaneously access the same CXL AIC, which limits overall system scalability.

To mitigate these bottlenecks, this study proposes a CXL-aware long-context LLM fine-tuning comprising two key components: (1) CXL-aware Memory Allocation, which strategically allocates offloaded data (model parameters, gradients, optimizer states) and activation values by considering their access patterns and latency sensitivity, thereby prioritizing memory placement according to specific workload requirements; and (2) Multi-AIC Striping, which allow CPU to leverage aggregated bandwidth of multiple CXL AICs and also alleviates bandwidth contention in multi-GPU system by distributing memory allocations across multiple CXL AICs. The multi-AIC striping method increases the available aggregate bandwidth and significantly reduces bottlenecks during intensive data transfer phases. Through these optimizations, this study demonstrates that CXL-attached memory can effectively enhance CPU offloading capabilities for long-context LLM fine-tuning, enabling training of larger models and handling longer contexts on resource-constrained hardware, while achieving performance comparable to configurations utilizing exclusively local DRAM. The main contributions are as follows.

1) To the best of our knowledge, this paper presents the first

detailed empirical study on the performance of CXL AIC memory specifically for long-context LLM fine-tuning with CPU offloading.

- 2) This study identifies and analyzes key performance bottlenecks introduced by naive CXL adoption.
- 3) The CXL-aware memory allocation is proposed to efficiently manage local DRAM and CXL-attached memory based on workload characteristics.
- 4) The multi-AIC striping mitigates bandwidth issues in multi-GPU setups and improves scalability.
- 5) Experimental results demonstrate that CXL-attached memory can sustain high performance, establishing CXL as a promising solution for next-generation AI workloads.

The remainder of the paper is structured as follows: Section II provides background and related work; Section III analyzes CXL-attached memory performance; Section IV details our proposed optimizations; Section V presents experimental evaluations; Section VI reports related works and Section VII concludes this study.

II. BACKGROUND

This section provides background on CPU offloading techniques for long-context LLM fine-tuning (See Section II-A), highlighting the associated system memory bottlenecks (See Section II-B) and the role of Compute Express Link (CXL) technology in addressing these limitations (See Section II-C).

A. CPU Offloading for Long-Context Fine-Tuning

ZeRO-Offload [20] is a widely used technique to train LLMs on systems with limited GPU memory. It conserves GPU resources by transferring model parameters, gradients, and optimizer states from GPU to system memory, and only retrieves them back to GPU memory when required for computation. To further reduce memory usage, ZeRO-Offload can be combined with techniques such as Flash-Attention [40, 41], Liger-Kernel [42], and gradient checkpointing (activation checkpointing) [17]. Flash-Attention efficiently computes attention without fully materializing the attention matrix, ensuring that peak memory scales linearly rather than quadratically with context length. Liger-Kernel optimizes large intermediate tensor usage during cross-entropy calculation by employing a FusedLinearCrossEntropy mechanism. Notably, the intermediate tensor usage also scales with context length and vocabulary size. Activation checkpointing reduces peak memory by storing only a subset of activations during the forward pass and recomputing them during the backward pass. Although these techniques significantly reduce GPU memory usage, they are still insufficient in long-context fine-tuning scenarios. This is because the size of checkpointed activations grows substantially with context length, making it necessary to offload them to system memory and retrieve them when needed [19]. Since model parameters, gradients, optimizer states, and checkpointed activations are all stored in system memory, the demand on system memory increases rapidly and can become a major bottleneck.

Figure 1 illustrates the aforementioned integrated approach, referred to as long-context CPU offloading with offloaded activation checkpointing, using a transformer model with four transformer blocks as an example. Each transformer block contains

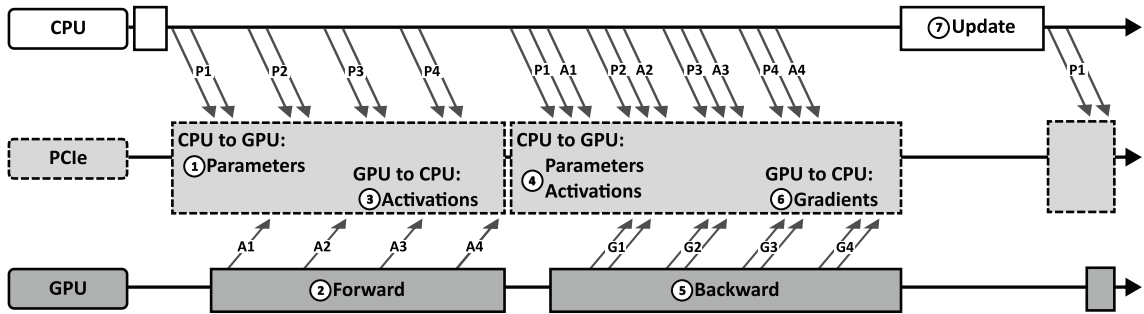


Fig. 1: Example of long-context CPU offloading with activation checkpointing with a transformer model composed of 4 transformer blocks. Arrows indicate data transfers over PCIe: P_i represent model parameters (e.g., attention projection parameters, feed-forward network parameters) for a specific block. A_i represent checkpointed input activations for block. G_i represent gradients corresponding to the parameters of block. The numbered steps illustrate the data movement and computation flow.

parameters for attention projections and feedforward layers. The workflow operates as follows: (1) First, necessary parameters are loaded from CPU to GPU memory on a tensor-by-tensor basis. (2) Next, the GPU performs forward computations using these parameters. (3) Checkpointed activations for each transformer block are offloaded to CPU memory. (4) Once the forward pass concludes, the backward pass requires parameters and previously checkpointed activations. (5) These data are then reloaded onto the GPU, which recomputes necessary activations to perform backpropagation. (6) Gradients computed on the GPU are subsequently offloaded to CPU memory, (7) enabling optimizer updates (e.g., using Adam) to execute entirely on the CPU after completing the backward pass. During optimizer steps, full precision parameters, optimizer states, and gradients reside primarily in CPU memory. Such an approach minimizes the volume of data transferred between the GPU and the CPU during each training iteration.

To clarify the memory footprint of the workflow shown in Figure 1, the GPU memory usage is first examined. During CPU offloading, the GPU is dedicated solely to computation and retains minimal data: model parameters are streamed block by block, and the corresponding activations and gradients are kept only until each block’s computation is complete. These are then immediately offloaded to system memory or discarded, shifting the primary memory burden to the system memory. On the other hand, the system memory usage is detailed in Table I. The upper half lists components frequently transferred between CPU and GPU during forward and backward passes, while the lower half lists components stored on the CPU for optimizer updates. The memory usage for model parameters and gradients depends on their precision: `bf16` requires 2 bytes per parameter, while `fp32` requires 4 bytes per parameter. For the Adam optimizer, the optimizer states (momentum and variance) require $8 \times P$ bytes in `fp32`, doubling the memory of gradients due to maintaining two states per parameter. For checkpointed activations, each GPU stores unique activations, scaled by N_g . Checkpoints are saved for each transformer block’s input, totaling L blocks, with each activation sized at $B \times C \times H$ elements, stored in `bf16` (2 bytes per element).

B. CPU Memory Bottleneck under Long-Context Offloading

In long-context CPU offloading scenarios, memory demand shifts predominantly from GPU memory to system memory. As

TABLE I: Breakdown of system memory components during CPU offloading. P : total parameters; N_g : number of GPUs; B : batch size per GPU; C : context length; L : number of transformer blocks; H : hidden size.

Component	Precision	Memory Usage (bytes)
Model parameters	<code>bf16</code>	$2 \times P$
Gradients	<code>bf16</code>	$2 \times P$
Checkpointed activations	<code>bf16</code>	$2 \times (N_g \cdot B \cdot C \cdot L \cdot H)$
Model parameters	<code>fp32</code>	$4 \times P$
Gradients	<code>fp32</code>	$4 \times P$
Optimizer states	<code>fp32</code>	$8 \times P$

a result, system memory capacity becomes a key factor in determining the feasible model size and the maximum context length. A larger system memory allows training with larger models, supports longer context windows, and enables sufficiently large batch sizes to achieve optimal performance. To illustrate this behavior, a motivational experiment was conducted using the 12B model to measure memory requirements and throughput across different context lengths and batch sizes in a 2-GPU setting (hardware specifications are listed in Table II). In the first part of the experiment, the batch size is fixed at 5, and the context length is varied from 512 to 32K tokens. The choice of 32K is based on previous long-context fine-tuning studies [11–15], which commonly use datasets with context lengths around 32K. For example, LongAlpaca [11] ranges from 3K to 9K, FILM [12] spans 4K to 32K, LongWriter [14] ranges from 2K to 32K, and LongAlign [15] ranges from 8K to 64K, with 90% of samples below 32K. In the second part, the context length is fixed at 4K, while the batch size is varied from 1 to 48 to observe changes in throughput and memory usage. The results are presented in Figures 2 and 3.

Figure 2 shows that CPU memory usage increases linearly with context length. This is because, in long-context CPU offloading, system memory needs to hold checkpointed activations, whose sizes scale proportionally with both the context length and the number of GPUs. Meanwhile, Figure 3 demonstrates that throughput improves with increasing batch size until saturation is reached. This suggests that once the model and context length are fixed, increasing the batch size can enhance GPU utilization. However, Figure 3 shows that CPU memory usage also increases linearly with batch size. This indicates

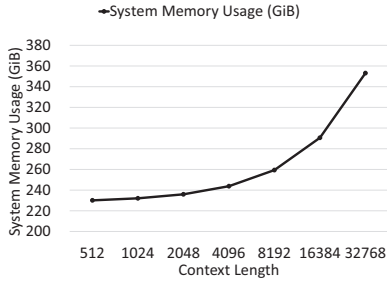


Fig. 2: System memory requirement scaling for 12B across varying context lengths with a batch size of 5.

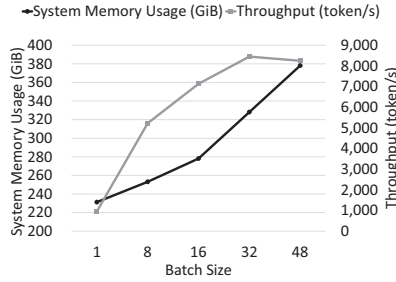


Fig. 3: Throughput and system memory requirement scaling for 12B across batch sizes with a 4K context length.

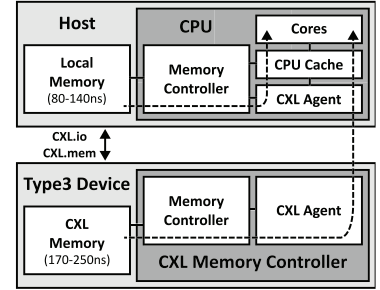


Fig. 4: Comparison of memory access data paths and latencies between local memory and CXL-attached memory

that memory demand is driven not only by model scale and context length but also by batch size when aiming for optimal performance. These findings highlight that in long-context CPU offloading scenarios, system memory usage increases and is likely to become a critical bottleneck as context lengths continue to grow.

C. CXL-Attached Memory

Compute Express Link (CXL) is built on top of PCIe and is designed to provide high-bandwidth, low-latency communication between the CPU (host) and various types of devices such as accelerators, memory expanders, and smart I/O devices. CXL differentiates devices into 3 types. Type 1 devices include accelerators with internal caches capable of directly caching host memory. Type 2 devices, such as GPUs, support mutual memory caching with the host, enabling unified memory access. Type 3 devices are intended for memory expansion and include components such as CXL-attached memory for expanding system memory capacity [26]. To enable the use cases of the above devices, three protocol sublayers, including CXL.io, CXL.cache, and CXL.mem, can be combined depending on the device type. While CXL.io provides traditional PCIe-like functionality for configuration, interrupts, and basic I/O operations, CXL.cache and CXL.mem enable devices to transparently cache host memory and allow the host to access memory attached to CXL devices, respectively.

For CXL-attached memory, Figure 4 illustrates the differences in data paths and latency between local and Type 3 devices. Accessing local memory follows a direct path from the CPU cores through the CPU cache and memory controller, resulting in latencies between 80 and 140 nanoseconds [27]. In contrast, accessing CXL-attached memory involves traversing the PCIe interface using the CXL.io and CXL.mem protocols. This path requires coordination between the CPU and the CXL memory controllers, leading to increased latency ranging from 170 to 250 nanoseconds [27]. While CXL-attached memory is utilized as a system memory extension, the Linux kernel integrates them as Non-Uniform Memory Access (NUMA) nodes [35]. This integration allows the system to manage CXL-attached memory within the existing memory management framework. Without manual intervention, the kernel uses NUMA policies to determine how memory is allocated across nodes. However, users can manually control memory allocation using tools like `numactl` and `libnuma` [43]. For example, a naive interleave

policy distributes memory pages in a round-robin fashion among available NUMA nodes [44]. Although existing integration effectively enlarges usable system memory, our investigation reveals that the performance of CPU-offloaded long-context LLM is suboptimal (See Section III).

III. CXL-ATTACHED MEMORY PERFORMANCE ANALYSIS

This section empirically characterizes the performance impact of storing CPU-offloaded data to CXL-attached memory. The naive deployment first prolongs CPU-based optimizer steps (See Section III-A) and induces severe bandwidth contention on the shared PCIe link in multi-GPU configurations (See Section III-B). These findings underscore the necessity of CXL-aware data-placement strategies (See Section III-C)

A. CPU-Offloading Slowdowns on CXL-Attached Memory

As illustrated in Section II-A, the long-context CPU-offloading workflow stores full-precision parameters, gradients, and optimizer states in system memory so that the CPU can perform the optimizer update locally. As each parameter update is independent, the optimizer phase exhibits ample parallelism. Practical implementations, such as ZeRO-Offload, exploit OpenMP threads and SIMD instructions (e.g., AVX2) to accelerate this compute-intensive step [20]. Consequently, the optimizer phase is highly parallelized and sensitive to increased latency when accessing offloaded data structures. To quantify how memory placement affects optimizer latency within the long-context CPU-offloading workflow, the CPU-based Adam optimizer is benchmarked with offloaded data structures residing either in local DRAM or in CXL-attached memory. Figure 5 summarizes the results. For each configuration, the data size is varied to emulate different LLM scales, excluding trivially small cases. Hardware details are listed in Table II with Config. A.

In Figure 5, an “element” consists of a 4 bytes parameter, a 4 bytes gradient, and 8 bytes of optimizer state. The SIMD kernel processes each element in three steps: (i) it loads the parameter, gradient, and state from memory into vector registers; (ii) executes the floating-point update; and (iii) writes the updated values back. For modest data volumes, the latency penalty of CXL-attached memory is negligible; however, once the element count exceeds roughly 20 million, optimizer time on CXL rises sharply, reaching nearly 4 times the DRAM baseline. The primary cause is the higher access latency of

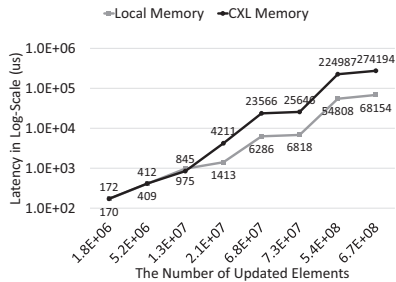


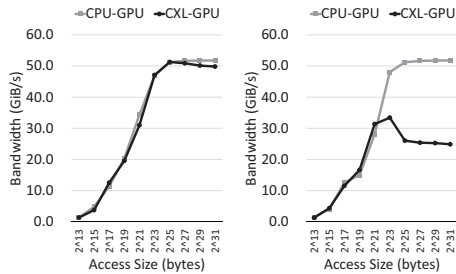
Fig. 5: Latency comparison of the CPU-Based Adam optimizer step.

the CXL path (170-250 ns) compared to local DRAM (80-140 ns), as shown earlier in Figure 4. These results indicate that naively placing latency-critical optimizer data in CXL-attached memory can severely degrade fine-tuning performance. Effective CXL deployments for long-context CPU-offloading need to keep latency-sensitive data in low-latency DRAM and relegate latency-tolerant data to CXL-attached memory, respectively.

B. GPU Data Transfers Slowdown on CXL-attached Memory

The CPU-offloading workflow described in Section II-A entails not only a CPU-intensive optimizer step but also frequent, high-volume data movement between system and GPU memory. Before each layer’s computation, model parameters and checkpointed activations are copied from system memory to the GPU; afterwards, the resulting gradients are copied back. To quantify how the physical location of the system memory influences these transfers, this section measures the GPU copy performance with source (or destination) buffers that reside in local DRAM or CXL-attached memory. For each experiment, page-aligned host buffers are allocated with `posix_memalign`, and `numactl` pins each allocation to the desired NUMA node—local DRAM or a CXL Type 3 AIC. The buffers are then registered with `cudaHostRegister`, enabling direct DMA over PCIe and avoiding extra copies through CPU caches. Asynchronous `cudaMemcpyAsync` transfers are issued via CUDA streams and events, while latency and effective bandwidth are recorded. Multi-GPU tests launch concurrent copy requests to both target GPUs. Hardware details are listed in Table II with Config. A. and PCIe Gen5 $\times 16$ link (128 GB/s bidirectional, 64 GB/s per direction) is utilized.

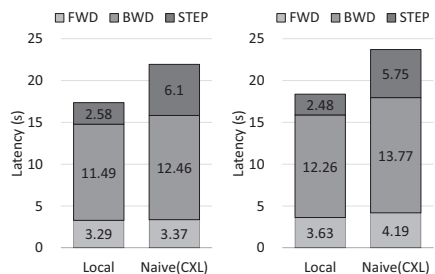
Results are presented in Figure 6. With a single GPU in Figure 6(a), transfer bandwidth from CXL-attached memory is virtually identical to that from local DRAM; throughput climbs with request size until it reaches the PCIe limit because page-locked buffers give both memory types an equivalent DMA path, making the operation interface-bound. A stark contrast emerges in the dual-GPU case, shown in Figure 6(b). When both GPUs copy concurrently, the aggregate bandwidth from the CXL AIC drops to roughly 25 GiB/s, which is far below the sum of two local DRAM transfers and well short of the theoretical link rate. The bottleneck is the single PCIe connection between the CXL AIC and the host; competing DMA streams must share this finite link, dramatically throttling each transfer. Local DRAM,



(a) Single GPU

(b) Dual GPU

Fig. 6: Bandwidth Comparison of System Memory to GPU Memory Transfers.



(a) Single GPU

(b) Dual GPU

Fig. 7: Latency breakdown of CPU offloading of local DRAM vs. CXL memory.

attached through the CPU’s memory controllers, avoids such shared-link contention.

Although these single-GPU results align with prior reports showing that CXL-to-GPU copies can rival local DRAM copies under isolated conditions [28,39], the multi-GPU results highlight a critical scaling limitation: *simultaneous GPU accesses to a single CXL AIC introduce severe bandwidth contention*, potentially negating the capacity benefits of CXL-attached memory in multi-GPU fine-tuning workflows.

C. Motivation: End-to-End Fine-Tuning Slowdown

Based on the characteristics outlined in previous sections, this section measures how naively incorporating CXL-attached memory affects end-to-end performance during LLM fine-tuning with CPU offloading. The comparison pits a local DRAM baseline against a configuration that combines local DRAM with CXL memory. Table II details the platform: one or two H100 GPUs fine-tuning a 12-billion-parameter model (4K context, batch size 16) while a single CXL Type 3 AIC contributes 512 GiB of capacity. Memory bindings were controlled with `numactl`: baseline runs allocated pages to the local DRAM NUMA node, whereas CXL runs naively round-robin interleaved allocations to the CXL NUMA node and the 128 GiB local DRAM NUMA node. Figure 7(a) presents the latency profile in the single-GPU scenario. The optimizer step (STEP phase) suffers the most because its CPU-bound loads and stores are acutely sensitive to the higher access latency of CXL memory, confirming the expectation from Section III-A. Phases dominated by GPU transfers (FWD, BWD) exhibit smaller slowdowns; prefetching and asynchronous DMA obscure part of the added latency.

Figure 7(b) shows that a dual-GPU configuration shifts the bottleneck. As predicted in Section III-B, concurrent traffic from both GPUs saturates the single AIC’s PCIe link, so the FWD and BWD phases degrade markedly, while STEP remains limited primarily by latency. Overall, naive CXL adoption introduces two principal issues: (1) substantial latency inflation during the optimizer step, and (2) severe bandwidth contention for GPU transfers in multi-GPU setups. These findings highlight the need for CXL-aware data-placement schemes that position parameters, gradients, optimizer states, and activations according to their sensitivity to latency versus bandwidth, as well as mechanisms that alleviate bandwidth contention across multiple GPUs. Properly addressing these challenges would let systems

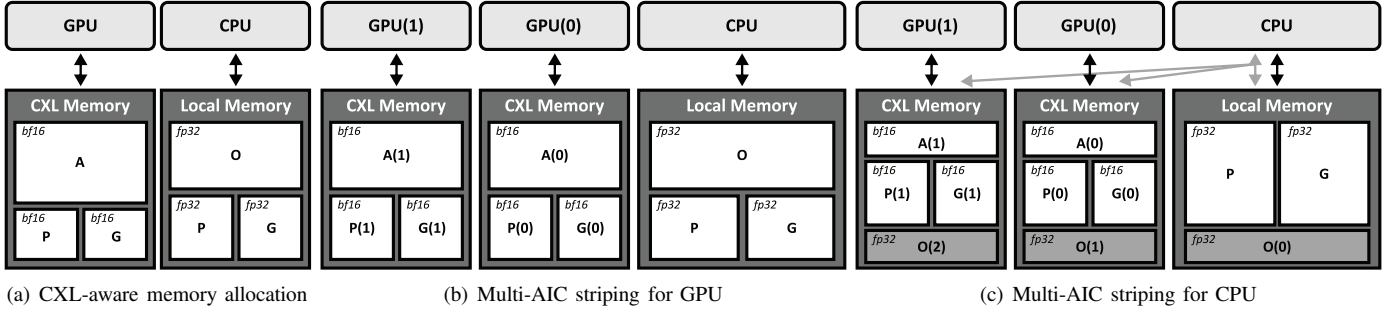


Fig. 8: Illustrative examples of CXL-aware allocation place latency-sensitive CPU compute data (full-precision P , G , O) in local DRAM and latency-tolerant GPU transfer data (A , P , G) in CXL-attached memory. And two Multi-AIC Striping scenarios, one for GPU-related to mitigate bandwidth contention. Another for striping CPU-computed data (e.g. full-precision O) across local DRAM and multiple CXL AICs to leverage aggregate memory capacity and bandwidth.

with modest local DRAM and ample CXL capacity fine-tune larger models and longer contexts without incurring prohibitive slowdowns.

IV. CXL-AWARE LONG-CONTEXT LLM FINE-TUNING

To curb the latency hit of CXL while still exploiting its capacity, the proposed CXL-aware long-context LLM fine-tuning first introduces the CXL-aware memory allocation to keep latency-critical optimizer data in DRAM and relegates bulky, latency-tolerant tensors to CXL memory (See Section IV-A). Complementing this, Multi-AIC striping spreads each GPU’s CXL-resident data across multiple add-in cards, eliminating single-link contention and pooling bandwidth, an approach that also scales when optimizer states spill beyond DRAM (See Section IV-B).

A. CXL-aware Memory Allocation

Building on the previous observations in Section III-A, the CXL-aware memory allocation is introduced to reserve local DRAM for the data most sensitive to latency during the CPU-based optimizer step, namely the full-precision model parameters P , gradients G , and optimizer states O . Data that tolerates higher latency, such as checkpointed activations A and bf16 copies of parameters and gradients streamed to the GPU, is directed to CXL-attached memory. This selective placement harnesses the greater capacity of CXL memory for storing latency-tolerant information without suffering the latency penalty of CXL-attached memory when latency-critical optimizer data reside on slower medium. Aligning each data type with the memory tier that best matches its access pattern not only improves efficiency but also enhances scalability for long-context workloads. As the context length or batch size expands, the footprint of the activation checkpoints A increases substantially (see Section II-B), while the sizes of P , G , and O remain fixed relative to the model parameters. Offloading the ever-increasing activation data to the expandable CXL pool alleviates pressure on local DRAM, enabling a stable DRAM configuration while relying on CXL for capacity growth. Figure 8(a) visualizes the memory layout, highlighting how each data component is distributed between local DRAM and CXL-attached memory.

B. Multi-AIC Striping

Even though CXL AICs make it straightforward to expand system memory capacity, effectively using multiple cards is still challenging. Earlier observations in Section III-B reveal severe bandwidth contention whenever several GPUs tried to access the same AIC. Additional profiling also showed that latency-tolerant transfer data—checkpointed activations A , parameters P , and gradients G benefit most from placement in CXL memory. Taken together, these findings motivate the multi-AIC striping approach, which splits each GPU process’s data across all available AICs, preventing concurrent traffic from piling onto a single card and relieving the observed bandwidth bottleneck. When the system contains more AICs than GPUs—for instance, one GPU paired with two AICs—the data is striped across all cards so transfers can harness their combined bandwidth. Figure 8(b) illustrates the arrangement for a two-GPU, two-AIC configuration.

Multi-AIC striping extends naturally to CPU-intensive phases. If the full-precision optimizer states O exceed local DRAM capacity, the data can be partitioned across both DRAM and the available AICs. During the optimizer step, the CPU accesses these partitions in parallel, drawing on the aggregate bandwidth of the local DRAM plus the CXL fabric. Figure 8(c) shows such a layout with two AICs. By distributing traffic across multiple cards, the strategy capitalizes on CXL’s aggregate bandwidth, improves scalability in GPU transfer phases, and alleviates memory-capacity pressure during CPU-bound steps.

V. EVALUATIONS

A. Experimental Setup

1) *Hardware and Software Specification*: Experiments run on a server whose hardware and software stack are summarized in Table II. The platform combines a high-performance CPU, ample local DRAM, and two cutting-edge GPUs optimized for LLM workloads. CXL memory expansion is evaluated in two configurations: a single-AIC setup and a dual-AIC setup designed to reveal scalability limits and bandwidth-contention effects. Both add-in cards were SMART Modular devices [30]. Notably, even though the current configuration is limited to the availability of CXL AICs, the observations made in this study are representative and transferable to other CXL configurations.

TABLE II: Hardware and Software Specification for Experimental Setup.

Component	Specification
<i>Hardware</i>	
OS	Ubuntu 24.04 LTS
Linux Kernel	v6.9
CPU	1 × Intel(R) Xeon(R) 6780E
GPUs	2 × NVIDIA H100 80GB PCIe
PCIe	PCIe 5.0 (x16 links for GPUs and AICs)
Local DRAM	512 GB (4 × 128 GB DDR5-6400)
CXL AICs. (Config. A)	1 × CXA-8F2W (512 GB AIC)
CXL AICs. (Config. B)	2 × CXA-4F1W (256 GB AIC)
<i>Software</i>	
NUMA Control	numactl, libnuma 2.0.19
PyTorch	torch 2.5.1
Model	transformers 4.47.1
Framework	deepspeed 0.16.2

2) *Workload Setup*: Data placement across local DRAM and CXL-attached memory is managed by `libnuma`, which is exposed to PyTorch through a custom extension. DeepSpeed [45], which is the implementation of ZeRO-Offload, handles CPU offloading, while Flash-Attention, Liger-Kernel, and activation checkpointing enable efficient long-context processing. Checkpointed activations, once generated, are offloaded to host DRAM. The study focuses on fine-tuning large language models under a Causal Language Modeling objective. Two representative models—**Qwen2.5-7B** [46] and **Mistral NeMo 12B** [47]—serve as workloads for exploring performance and scalability across varying context lengths, batch sizes, GPU counts, and AIC configurations. All experiments employ `bf16` mixed-precision training. The Adam optimizer maintains `fp32` master parameters and optimizer states on the CPU, delivering the numerical stability required for LLM fine-tuning. Details on specific context lengths, batch sizes, and AIC setups appear in the individual results subsections.

B. Performance Evaluation with a Single CXL AIC

The single-AIC scenario, corresponding to Config. A in Table II, serves as the starting point. Three configurations quantify the impact of adopting CXL-attached memory: (1) **Baseline**, where all data reside in local DRAM; (2) **Naive CXL**, which combines 128 GiB of local DRAM with 512 GiB of CXL memory under a naive `numactl` interleave-all policy; and (3) **Our CXL**, which pairs the same capacities while applying the proposed CXL-aware Memory Allocation strategy. Figure 9(a) reports single-GPU throughput for a 7B model across context lengths from 4K to 32K and batch sizes from 1 to 32. Relative to the baseline (normalized to 100%), the naive CXL setup drops to roughly 76%–94%. Degradation varies with workload mix: scenarios dominated by forward (FWD) and backward (BWD) passes suffer less because the latency-critical optimizer step (STEP) forms a smaller share of runtime. Applying CXL-aware allocation restores throughput to about 97%–99%, eliminating most of the loss. In other words, the corresponding performance drop is only 1% - 3% compared to the DRAM-only baseline and improved from the naive CXL by up to 21%.

Figure 9(b) shows analogous results for a 12 B model. The naive CXL configuration falls to roughly 72%–93% of the base-

line, whereas the CXL-aware method climbs to approximately 88%–96%. Even with the larger model pressing local memory to its limits, the drop remains confined to 4%–12%, a clear improvement over the naive policy. Dual-GPU results appear in Figure 9(c) for both 7B and 12B models. Performance under the naive CXL policy reaches only 84%–94% of the baseline, while CXL-aware allocation raises that range to 86%–99%. Although the gains are smaller than in single-GPU trials—bandwidth contention still exists when two GPUs share a single AIC—the drop is limited to 1%–14%, depending on model size and context length. Multi-AIC Striping, discussed next, addresses this remaining bottleneck by distributing traffic across multiple cards.

C. Performance Evaluation with a Dual CXL AIC

The evaluation next turns to the dual-AIC scenario, designated Config. B in Table II. Three configurations establish the impact of CXL memory: (1) **Baseline**, where all data remain in local DRAM; (2) **Naive CXL**, which pairs 128 GiB of DRAM with two 256 GiB AICs under a naive `numactl` interleave-all policy; and (3) **Our CXL**, which uses the same capacities but applies CXL-aware Memory Allocation plus Multi-AIC Striping.

Figure 10(a) presents single-GPU throughput for a 12B model across the same range of context lengths and batch sizes used earlier. Naive CXL drastically reduces throughput, delivering a reduction 2% - 11% of baseline performance. In contrast, CXL-aware allocation combined with Multi-AIC Striping restores the speed to 100% - 101% of the baseline, proving that dual cards can fully recover and slightly exceed native DRAM performance when bandwidth is balanced correctly. Figures 10(b) and 10(c) extend the study to dual-GPU training of 7 B and 12 B models. Under the naive policy, throughput again reduces 2%–9% of the baseline. Introducing CXL-aware allocation together with striping trims performance by at most 1%, effectively matching the DRAM-only baseline even while two GPUs share system memory.

Earlier single-AIC experiments showed limited gains because alone card became a bandwidth bottleneck. Dual-AIC striping eliminates this constraint by distributing traffic, allowing CPU and GPU workloads to exploit the aggregate bandwidth of both cards. *The resulting speedups over both single-AIC tests and naive dual-AIC adoption underline the importance of coordinated data placement and balanced striping when scaling CXL-based memory expansion.*

VI. RELATED WORKS

Offloading strategies have emerged as an effective way to break the GPU memory ceiling, enabling the training of models that would otherwise exceed on-device capacity by staging tensors in CPU DRAM or NVMe SSDs [20–24]. Among these, the ZeRO series [20, 21] has become the most widely adopted, thanks to continuous maintenance that fixes bugs, adds support for new models, and preserves interoperability with complementary optimizations such as Flash-Attention [40] and Liger-Kernel [42]. Its reference implementation now underpins popular training frameworks, including Accelerate [48] and MS-Swift [49]. Complementary research broadens the design space of memory-centric training. Huan et al. [22] tailor an

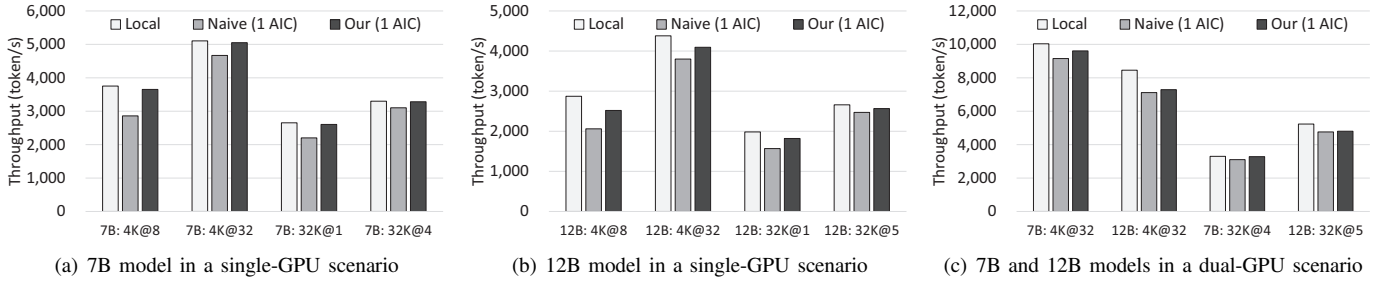


Fig. 9: Training throughput comparison for three configurations: (1) Baseline (using local DRAM only), (2) Naive CXL adoption for single AIC, and (3) Using CXL-attached memory with CXL-aware Memory Allocation for single AIC. Performance is shown across varying context lengths and batch sizes for each scenario.

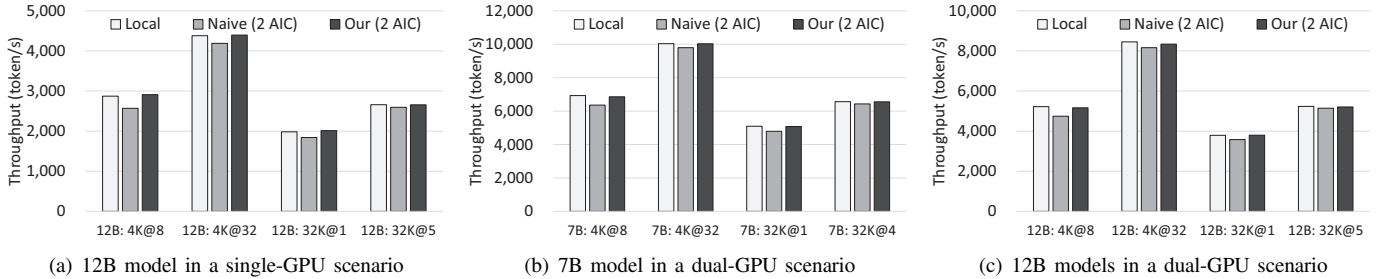


Fig. 10: Training throughput comparison for three configurations: (1) Baseline (using local DRAM only), (2) Naive CXL adoption for dual AICs, and (3) Using CXL-attached memory with CXL-aware Memory Allocation and Multi-AIC Striping for dual AICs. Performance is shown across varying context lengths and batch sizes for each scenario.

offloading mechanism specifically for large-scale language models, while Chen et al. [23] evaluate pragmatic orchestration policies that coordinate CPU and GPU memory during fine-tuning. Zeng et al. [24] further extend the idea to fully heterogeneous environments, automatically balancing both compute and memory resources.

For CXL-attached memory, several tiered-memory systems (TMS) tackle the same capacity challenge at the operating system level. Maruf et al.’s TPP [34] classifies pages as hot or cold and places them in the most appropriate tier, keeping latency-critical data in DRAM and relegating infrequently accessed data to CXL-attached memory. Xiang et al.’s NOMAD [50] augments Linux with transactional page migration and page shadowing, permitting a page to be present in fast and slow memory simultaneously and moving it asynchronously outside the application’s critical path. Workload-aware refinements continue to emerge. Vuppapapati et al. [51] observe that DRAM latency can spike near bandwidth saturation, sometimes exceeding that of CXL memory; their Colloid policy dynamically balances traffic across tiers to equalize effective access latency. San et al.’s M5 [52] embeds FPGA-based hot-page and hot-word trackers in the CXL controller, supplying fine-grained access statistics with negligible overhead. General-purpose TMS designs operate transparently and require no application changes, yet this very neutrality can leave performance on the table for specialized workloads.

VII. CONCLUSION

To address the challenges of high latency and limited bandwidth in CXL-attached memory compared to local DRAM during long-context LLM fine-tuning, particularly the performance

degradation in CPU-intensive computations and the bandwidth contention among multiple GPUs, this study is among the first to propose two key approaches. First, CXL-aware memory allocation strategically places latency-sensitive data in local DRAM and latency-tolerant data in CXL-attached memory based on access patterns. Second, multi-AIC striping distributes data across multiple CXL AICs to aggregate bandwidth, benefiting CPU-intensive phases and multi-GPU configurations. These optimizations significantly mitigate the performance drawbacks of CXL-attached memory, consistently outperforming naive CXL adoption with improvements ranging up to 21% in various scenarios. In particular, in the dual AIC configuration, our approach retains near-baseline performance, reducing the performance gap between DRAM-only setups to just 1% at most. These results demonstrate that this study enables CXL-attached memory as a viable solution for long-context LLM fine-tuning.

REFERENCES

- [1] S. Minaee, T. Mikolov, N. Nikzad *et al.*, “Large language models: A survey,” *arXiv preprint arXiv:2402.06196*, 2025. [Online]. Available: <https://arxiv.org/abs/2402.06196>
- [2] J. Liu, D. Zhu, Z. Bai *et al.*, “A comprehensive survey on long context language modeling,” *arXiv preprint arXiv:2503.17407*, 2025. [Online]. Available: <https://arxiv.org/abs/2503.17407>
- [3] DeepSeek-AI, D. Guo, D. Yang *et al.*, “Deepseek-r1: Incentivizing reasoning capability in llms via reinforcement learning,” DeepSeek-AI, Tech. Rep., 2025. [Online]. Available: <https://arxiv.org/abs/2501.12948>
- [4] OpenAI. (2024) Learning to reason with llms. [Online]. Available: <https://openai.com/index/learning-to-reason-with-llms/>
- [5] —. (2025) Introducing deep research. [Online]. Available: <https://openai.com/index/introducing-deep-research/>
- [6] G. Team, P. Georgiev, V. I. Lei *et al.*, “Gemini 1.5: Unlocking multimodal understanding across millions of tokens of context,” *arXiv preprint arXiv:2403.05530*, 2024. [Online]. Available: <https://arxiv.org/abs/2403.05530>

- [7] J. Lee, A. Chen, Z. Dai *et al.*, “Can long-context language models subsume retrieval, rag, sql, and more?” *arXiv preprint arXiv:2406.13121*, 2024. [Online]. Available: <https://arxiv.org/abs/2406.13121>
- [8] L. Wang, N. Yang, X. Huang *et al.*, “Large search model: Redefining search stack in the era of llms,” *SIGIR Forum*, 2024. [Online]. Available: <https://doi.org/10.1145/3642979.3643006>
- [9] Qwen. (2025) Qwen2.5 vl. [Online]. Available: <https://qwenlm.github.io/blog/qwen2.5-vl/>
- [10] Y. Weng, M. Han, H. He, X. Chang, and B. Zhuang, “Longvlm: Efficient long video understanding via large language models,” *arXiv preprint arXiv:2404.03384*, 2024. [Online]. Available: <https://arxiv.org/abs/2404.03384>
- [11] Y. Chen, S. Qian, H. Tang *et al.*, “Longlora: Efficient fine-tuning of long-context large language models,” *arXiv preprint arXiv:2309.12307*, 2024. [Online]. Available: <https://arxiv.org/abs/2309.12307>
- [12] S. An, Z. Ma, Z. Lin, N. Zheng, and J.-G. Lou, “Make your llm fully utilize the context,” in *Advances in Neural Information Processing Systems*, 2024. [Online]. Available: https://proceedings.neurips.cc/paper_files/paper/2024/file/71c3451f6cd6a4f82bb822db25cea4fd-Paper-Conference.pdf
- [13] J. Zhang, Y. Bai, X. Lv *et al.*, “Longcite: Enabling llms to generate fine-grained citations in long-context qa,” *arXiv preprint arXiv:2409.02897*, 2024. [Online]. Available: <https://arxiv.org/abs/2409.02897>
- [14] Y. Bai, J. Zhang, X. Lv *et al.*, “Longwriter: Unleashing 10,000+ word generation from long context llms,” *arXiv preprint arXiv:2408.07055*, 2024. [Online]. Available: <https://arxiv.org/abs/2408.07055>
- [15] Y. Bai, X. Lv, J. Zhang *et al.*, “Longalign: A recipe for long context alignment of large language models,” *arXiv preprint arXiv:2401.18058*, 2024. [Online]. Available: <https://arxiv.org/abs/2401.18058>
- [16] Y. Li, A. Phanishayee, D. Murray, J. Tarnawski, and N. S. Kim, “Harmony: overcoming the hurdles of gpu memory capacity to train massive dnn models on commodity servers,” *Proceedings of the VLDB Endowment*, 2022. [Online]. Available: <http://dx.doi.org/10.14778/3551793.3551828>
- [17] T. Chen, B. Xu, C. Zhang, and C. Guestrin, “Training deep nets with sublinear memory cost,” *arXiv preprint arXiv:1604.06174*, 2016. [Online]. Available: <https://arxiv.org/abs/1604.06174>
- [18] V. A. Korthikanti, J. Casper, S. Lym *et al.*, “Reducing activation recomputation in large transformer models,” in *Proceedings of Machine Learning and Systems*, 2023. [Online]. Available: https://proceedings.mlsys.org/paper_files/paper/2023/file/80083951326cf5b35e5100260d64ed81-Paper-mlsys2023.pdf
- [19] Unsloth. (2025) Unsloth gradient checkpointing - 4x longer context windows. [Online]. Available: <https://unsloth.ai/blog/long-context>
- [20] J. Ren, S. Rajbhandari, R. Y. Aminabadi *et al.*, “Zero-offload: Democratizing billion-scale model training,” in *2021 USENIX Annual Technical Conference (USENIX ATC 21)*, 2021.
- [21] S. Rajbhandari, O. Ruwase, J. Rasley *et al.*, “Zero-infinity: Breaking the gpu memory wall for extreme scale deep learning,” in *Proceedings of the international conference for high performance computing, networking, storage and analysis*, 2021.
- [22] H. Huang, J. Fang, H. Liu, S. Li, and Y. You, “Elixir: Train a large language model on a small gpu cluster,” *arXiv preprint arXiv:2212.05339*, 2023. [Online]. Available: <https://arxiv.org/abs/2212.05339>
- [23] S. Chen, Z. Wang, Z. Guan *et al.*, “Practical offloading for fine-tuning llm on commodity gpu via learned sparse projectors,” in *Proceedings of the AAAI Conference on Artificial Intelligence*, 2025.
- [24] Z. Zeng, C. Liu, X. He, J. Hu, Y. Jiang, F. Huang, K. Li, and W. Y. B. Lim, “Autohete: An automatic and efficient heterogeneous training system for llms,” *arXiv preprint arXiv:2503.01890*, 2025. [Online]. Available: <https://arxiv.org/abs/2503.01890>
- [25] AMD. (2025) Amd ryzen™ 9 9950x3d gaming and content creation processor. [Online]. Available: <https://www.amd.com/en/products/processors/desktops/ryzen/9000-series/amd-ryzen-9-9950x3d.html>
- [26] CXL. (2025) Cxl® specification. [Online]. Available: <https://computeexpresslink.org/cxl-specification/>
- [27] C. Chen, X. Zhao, G. Cheng *et al.*, “Next-gen computing systems with compute express link: a comprehensive survey,” *arXiv preprint arXiv:2412.20249*, 2025. [Online]. Available: <https://arxiv.org/abs/2412.20249>
- [28] X. Wang, J. Liu, J. Wu *et al.*, “Exploring and evaluating real-world cxl: Use cases and system adoption,” *arXiv preprint arXiv:2405.14209*, 2025. [Online]. Available: <https://arxiv.org/abs/2405.14209>
- [29] Micron. (2025) Micron memory expansion module using cxl. [Online]. Available: <https://www.micron.com/products/memory/cxl-memory>
- [30] S. Modular. (2025) Cxl memory. [Online]. Available: <https://www.smartm.com/product/list/cxl-memory>
- [31] ——. (2025) For memory expansion and memory pooling. [Online]. Available: <https://www.smartm.com/product/promote/compute-express-link>
- [32] Micron, “Cxl memory expansion: a closer look on actual platform,” Micron, Tech. Rep., 2025. [Online]. Available: <https://www.micron.com/content/dam/micron/global/public/products/white-paper/cxl-memory-expansion-a-close-look-on-actual-platform.pdf>
- [33] Y. Sun, J. Kim *et al.*, “M5: Mastering page migration and memory management for cxl-based tiered memory systems,” in *Proceedings of the 30th ACM International Conference on Architectural Support for Programming Languages and Operating Systems, Volume 2*, ser. ASPLOS ’25, 2025. [Online]. Available: <https://doi.org/10.1145/3676641.3711999>
- [34] H. A. Maruf, H. Wang, A. Dhanotia *et al.*, “Tpp: Transparent page placement for cxl-enabled tiered-memory,” in *Proceedings of the 28th ACM International Conference on Architectural Support for Programming Languages and Operating Systems, Volume 3*, ser. ASPLOS ’23. ACM, 2023. [Online]. Available: <http://dx.doi.org/10.1145/3582016.3582063>
- [35] Linux. Numa memory policy. [Online]. Available: https://www.kernel.org/doc/html/v6.9/admin-guide/mm/numa_memory_policy.html
- [36] J. Jang, H. Choi, H. Bae *et al.*, “CXL-ANNS: Software-Hardware collaborative memory disaggregation and computation for Billion-Scale approximate nearest neighbor search,” in *2023 USENIX Annual Technical Conference (USENIX ATC 23)*, 2023. [Online]. Available: <https://www.usenix.org/conference/atc23/presentation/jang>
- [37] M. Arif, K. Assogba, M. M. Rafique, and S. Vazhkudai, “Exploiting cxl-based memory for distributed deep learning,” in *Proceedings of the 51st International Conference on Parallel Processing*, ser. ICPP ’22, 2023. [Online]. Available: <https://doi.org/10.1145/3545008.3545054>
- [38] M. Kwon, J. Jang, H. Choi, S. Lee, and M. Jung, “Failure tolerant training with persistent memory disaggregation over cxl,” *IEEE Micro*, 2023.
- [39] Y. Tang, R. Cheng, P. Zhou *et al.* Exploring cxl-based kv cache storage for llm serving. [Online]. Available: <https://mlforsystems.org/assets/papers/neurips2024/paper17.pdf>
- [40] T. Dao, D. Fu, S. Ermon, A. Rudra, and C. Ré, “Flashattention: Fast and memory-efficient exact attention with io-awareness,” *Advances in neural information processing systems*, 2022.
- [41] T. Dao, “Flashattention-2: Faster attention with better parallelism and work partitioning,” *arXiv preprint arXiv:2307.08691*, 2023. [Online]. Available: <https://arxiv.org/abs/2307.08691>
- [42] P.-L. Hsu, Y. Dai, V. Kothapalli *et al.*, “Liger kernel: Efficient triton kernels for llm training,” *arXiv preprint arXiv:2410.10989*, 2025. [Online]. Available: <https://arxiv.org/abs/2410.10989>
- [43] numactl. Numa support for linux. [Online]. Available: <https://github.com/numactl/numactl>
- [44] Linux. numactl(8) - linux man page. [Online]. Available: <https://linux.die.net/man/8/numactl>
- [45] Microsoft. DeepSpeed. [Online]. Available: <https://www.deepspeed.ai/>
- [46] Qwen, :, A. Yang, B. Yang *et al.*, “Qwen2.5 technical report,” *arXiv preprint arXiv:2412.15115*, 2025. [Online]. Available: <https://arxiv.org/abs/2412.15115>
- [47] MistralAI and NVIDIA. Mistral nemo. [Online]. Available: <https://mistral.ai/news/mistral-nemo>
- [48] S. Gugger, L. Debut, T. Wolf *et al.* (2022) Accelerate: Training and inference at scale made simple, efficient and adaptable. <https://github.com/huggingface/accelerate>.
- [49] Y. Zhao, J. Huang, J. Hu *et al.*, “Swift: a scalable lightweight infrastructure for fine-tuning,” in *Proceedings of the AAAI Conference on Artificial Intelligence*, 2025.
- [50] L. Xiang, Z. Lin, W. Deng *et al.*, “Nomad: Non-Exclusive memory tiering via transactional page migration,” in *18th USENIX Symposium on Operating Systems Design and Implementation (OSDI 24)*, 2024. [Online]. Available: <https://www.usenix.org/conference/osdi24/presentation/xiang>
- [51] M. Vuppalaapati and R. Agarwal, “Tiered memory management: Access latency is the key!” in *Proceedings of the ACM SIGOPS 30th Symposium on Operating Systems Principles*, 2024. [Online]. Available: <https://doi.org/10.1145/3694715.3695968>
- [52] Y. Sun, J. Kim, Z. Yu *et al.*, “M5: Mastering page migration and memory management for cxl-based tiered memory systems,” in *Proceedings of the 30th ACM International Conference on Architectural Support for Programming Languages and Operating Systems, Volume 2*, 2025. [Online]. Available: <https://doi.org/10.1145/3676641.3711999>